Monte Carlo Study of the Anisotropic Three-Dimensional Heisenberg Model in a Crystal Field

R. T. S. Freire, J. A. Plascak, and B. V. da Costa

Departamento de Física, ICEx, Universidade Federal de Minas Gerais

Caixa Postal 702, 30123-970 Belo Horizonte, MG, Brasil

We study the phase diagram of the three-dimensional classical ferromagnetic Heisenberg model with an easy-plane crystalline anisotropy and an easy-axis exchange anisotropy through Monte Carlo simulations. We employ the Metropolis algorithm together with single-histogram techniques in order to characterize the transitions in each region of the phase diagram. Our results reveal, besides the disordered phase, the existence of Ising-like and XY-like ordered phases which are separated by a first-order transition line.

1 Introduction

Much work has been done on two- or three-dimensional Heisenberg models submitted to exchange or crystalline anisotropies [1-5]. However, as far as we know, much less work has been performed concerning the Heisenberg model submitted to both exchange and crystalline anisotropies. In this paper we focus our attention on the three-dimensional classical ferromagnetic Heisenberg model taking into account the competition between these different kinds of anisotropies and determining the phase diagram of the system.

The anisotropic Heisenberg model in a crystal field can be described by the Hamiltonian

$$H = -J \sum_{<i,j>} \vec{S}_i \cdot \vec{S}_j - A \sum_{<i,j>} S_i^z S_j^z + D \sum_i (S_i^z)^2, \quad (1)$$

where J, A, D are non-negative coupling constants and $<i,j>$ means a sum over nearest neighbor spins (in what follows we set $J = 1$). The second term is related to the exchange anisotropy and behaves as an easy-axis anisotropy since it tends to align the spins in the z direction in order to lower the energy of the system. The third term, on the contrary, corresponds to the crystalline, easy-plane anisotropy, which favors the spin alignment in the XY plane. We have, thus, a competition between the exchange anisotropy, which induces an Ising-like ordering, and the crystal field, which induces an XY-like ordering. Consequently, one expects a crossover from an Ising-like to an XY-like behavior for some special combination of A and D. In fact, it can be shown that, at zero temperature, two different phases coexist for D=3A namely, one with all the spins aligned in the z-direction and another one with all spins aligned along an arbitrary direction in the $x - y$ plane. It is the purpose of this work to study the phase diagram of this model as a function of the parameters of the Hamiltonian and locate not only the first-order transition line at finite low temperatures, but also the

second-order lines, separating these ordered phases from the disordered one, that appears at high temperatures. In the next section we present some details of the simulations and the quantities we have computed from them. The results are discussed in section 3 and the conclusions are given in the final section.

2 Simulational methods

In order to study the model above we performed Monte Carlo simulations [6, 7] and computed the specific heat

$$c_V = L^3 \frac{(<E^2> - <E>^2)}{T^2}, \quad (2)$$

the magnetic susceptibility

$$\chi = L^3 \frac{(<m^2> - <m>^2)}{T}, \quad (3)$$

and its z-component

$$\chi_z = L^3 \frac{(<m_z^2> - <m_z>^2)}{T}, \quad (4)$$

where E is the energy per spin, and $m = \frac{1}{L^3} \sum_i^{L^3} S_i$ and $m_z = \frac{1}{L^3} \sum_i^{L^3} S_i^z$ are the total magnetization and its z-component, respectively. The mean value of a quantity A is given by

$$<A> = \frac{1}{N - N_0} \sum_{j>N_0}^N A_j, \quad (5)$$

where N_0 is the number of Monte Carlo steps per spin (MCS) used for equilibration and N is the total number of MCS. In the definitions above, we have also set $k_B = 1$.

The global phase diagram is obtained through the location of the maxima of the specific heat and the magnetic susceptibilities. We consider finite $L \times L \times L$ lattices with periodic boundary conditions. To locate the maxima we performed preliminary simulations for each value of the parameters, using a temperature step $\Delta T = 0.1$ and $N_o = 100 \times L^2$ Monte Carlo steps per site for the system to achieve thermal equilibrium at the lower, initial temperature. For the subsequent temperatures, we used the final configuration of the previous temperature as the initial configuration for the next one and $N_o = 3000$ MCS for reaching the new equilibrium state. Following equilibration, runs comprising up to 3×10^4 MCS were performed in order to evaluate the corresponding thermodynamic quantities. Once we get the approximate location of the maximum from this preliminary simulation, we performed another one in the vicinity of the peak using $\Delta T = 0.01$ with runs comprising now up to 10^5 MCS. This procedure has been done considering a particular lattice size, namely $L = 14$. However, we have also done a finite-size scaling analysis [6-9] at some specific values of the parameters by taking $L = 10, 12, 14, 16$ for second-order transitions and $L = 12, 14, 16, 20, 24$ for first-order transitions and using the single histogram re-weighting technique[10]. In this case the histograms have been taken with 10^6 MCS for second-order and 2×10^6 MCS for first-order transitions. From this approach we were able to obtain a more precise value for the transition temperatures, as well as critical exponent ratios. We have nevertheless observed that the extrapolated transition temperatures were very close to the value obtained for $L = 14$ (a discrepancy of less than 2%).

3   Results

We determine the properties of the system defined by the Hamiltonian of Eq. (1) using the methods described in the previous section. We considered first $A = 1$. Apart from the finite-size scaling analysis, all the curves were obtained taking $L = 14$. To show the competition between anisotropies, Figure 1 illustrates the temperature dependence of the z-component of the magnetic susceptibility and total magnetic susceptibility for different values of the parameter D.

In both cases, we observe that the peaks initially move towards smaller temperatures with increasing D (see Figs. 1(a) and 1(c)). For $D \approx 3.5$, a secondary peak appears, although more distinctively in the z-component of the magnetic susceptibility. With further increase of D (Figs. 1(b) and 1(d)), this secondary peak travels towards higher temperatures, in opposition to the primary peak, in such a way that they coalesce for $D \approx 4.0$. From this value on just one peak going to higher temperatures is observed in the magnetic susceptibility. For the z-component of the magnetic susceptibility, this peak progressively fades away as D continues to increase. A similar behavior is observed in the specific heat. Associating these maxima to the phase transition we are able to plot the phase diagram for the model as in Fig. 2. This diagram reveals an Ising-like region, separated from an XY-like region by a first-order transition line. Both ordered phases are separated from the paramagnetic phase
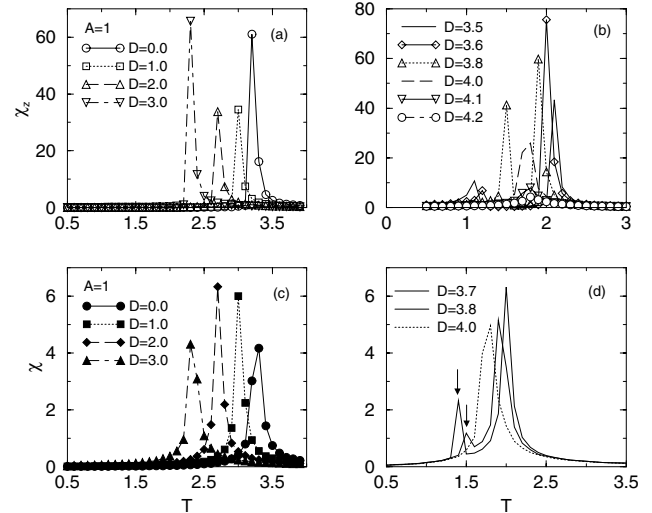
by second-order transition lines.

Figure 1.   Behavior of the magnetic susceptibility and its z-component as a function of temperature for various values of D for $A = 1$ and $L = 14$. In (d) the arrows indicate the position of the secondary peaks and the symbols have been suppressed for the sake of clarity.
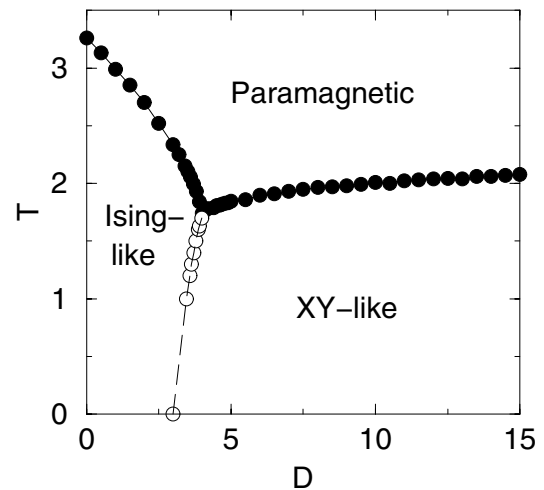

Figure 2. Phase diagram for the model given by Eq. (1). Here $A = 1$ and $L = 14$. Full circles represent second-order and open circles first-order transitions. The lines are guides to the eyes and meet at a bicritical point. The error bars are of the same order as the symbol sizes and have been omitted for clarity.

In order to characterize the order of the transitions we have done a finite-size scaling analysis with the use of single histogram re-weighting techniques. Fig. 3 shows the scaling behavior of the maximum of the magnetic susceptibility for $D = 0$ and $D = 3$ (on the Ising-like boundary) and $D = 6$ and $D = 8$ (on the XY-like boundary). One can see an expected second-order scaling behavior with $\gamma/\nu = 2.05(6)$ for $D = 0$ and $\gamma/\nu = 2.08(6)$ for $D = 3$ at the Ising-like boundary. As for the XY-like boundary one has $\gamma/\nu = 2.12(6)$ and $\gamma/\nu = 2.13(6)$ for $D = 6$ and $D = 8$, respectively. Although the present approach is inadequate to discriminate between the ratio γ/ν of the three-dimensional Ising and XY universality classes

(namely, $\gamma/\nu = 1.970(9)$ and $1.97(1)$[11], respectively) a clear universal second-order transition is observed for these lines at high temperatures. A finite-size scaling analysis of the critical temperature is shown in Figure 4 for several values of D along the second-order lines. One can notice again a clear second-order scaling behavior with the extrapolated temperatures very close to those obtained by just taking $L = 14$. These results justify the use of $L = 14$ in order to obtain the phase diagram depicted in Figure 2.
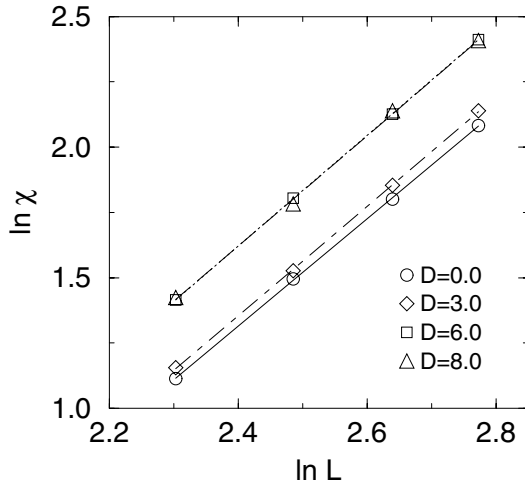
Figure 3. Finite-size scaling analysis of the maximum of the total magnetic susceptibility for particular points on the Ising-like ($D = 0$ and $D = 3$) and XY-like ($D = 6$ and $D = 8$) boundaries.
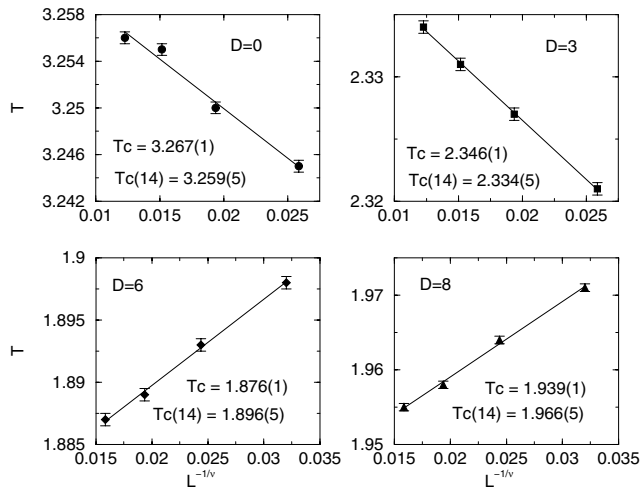

Figure 4. Finite-size scaling for the temperature and various values of D along the second-order transition lines. T_c means the extrapolated temperature and $T_c(14)$ is the corresponding value for lattice size $L = 14$. For $D = 0$ and $D = 3$ we have used $\nu_{Ising} = 0.630$ and for $D = 6$ and $D = 8$, $\nu_{XY} = 0.669$.
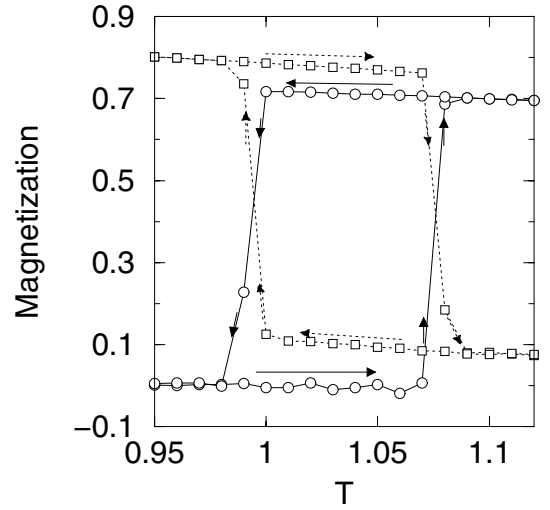

Figure 5. Temperature dependence of the z and xy components of the magnetization in the low temperature region for $D = 3.5$, $A = 1$ and $L = 14$. Increasing and decreasing temperatures are indicated by the arrows. The two different hysteresis curves are apparent from this figure. Open circles represent m_z and open squares m_{xy}.
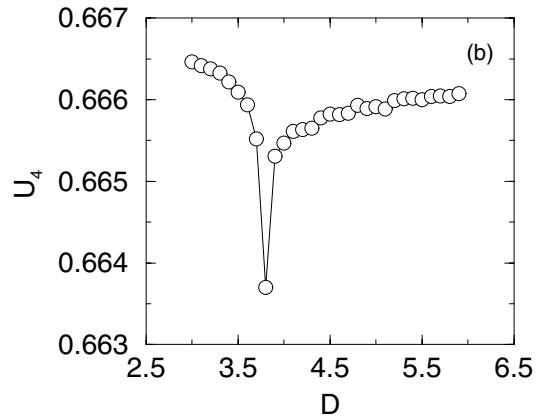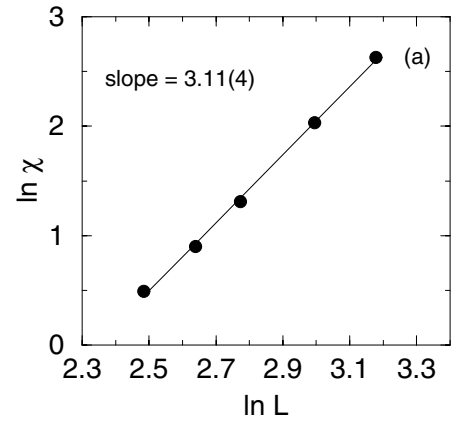

Figure 6. Characterization of the first-order transition line. (a) Finite-size scaling analysis of the maximum of the total magnetic susceptibility for a particular point on the first-order transition line namely, $D = 3.8$ and $T = 1.5$. The errors are smaller than the symbol sizes. (b) Fourth-order cumulant as a function of D for $T = 1.5$ and $L = 14$. The behavior of this quantity also indicates the occurrence of a first-order phase transition.

A different behavior occurs at low temperatures. Fig. 5 shows the behavior of the z and xy components of the magnetization as a function of temperature for $D = 3.5$ and $0.95 \leq T \leq 1.12$ i.e., crossing the first-order boundary. For $T \sim 0.95$ one has $m_z \sim 0$ and a finite value of m_{xy}, characterizing the XY-like phase. On the other hand, for $T \sim 1.1$ the opposite occurs with $m_{xy} \sim 0$ and a finite m_z, characterizing thus the Ising-like phase. The hysteresis in both magnetization curves is apparent from this figure. We have also done a finite-size scaling analysis of the maximum of the susceptibility for $D = 3.8$ on this boundary line. The results are shown in Fig. 6(a) with a slope of $3.11(4)$, which is reasonably close to the expected value $d = 3$ for a first-order phase transition [9]. In addition, Fig. 6(b) also shows the fourth-order magnetization cumulant as a function of D for $T = 1.5$, which exhibits a minimum around $D = 3.8$, corresponding in fact to the transition value. From the results above the first-order character of this transition line is clear.

4   Conclusions

In this work we have studied the phase diagram of the three-dimensional anisotropic Heisenberg model in a crystal field by means of Monte Carlo simulations. We have shown that the phase diagram presents, besides the disordered phase at high temperatures, an XY-like and an Ising-like phase at low temperatures. Both ordered phases undergo a second-order phase transition to the disordered phase and are separated by a first-order boundary. These lines meet at a bicritical point given by $T = 1.73(3)$ and $D = 3.95(4)$. A similar picture is observed for other values of A, with the bicritical point moving towards smaller T and D as A decreases. For instance, for $A = 0.5$ one has the bicritical point at $T = 1.68(4)$ and $D = 2.00(3)$.

References

[1] B. V. Costa and A.S.T. Pires, J. Mag. and Mag. Mat. **262**(2), 316 (2003).

[2] R. van de Kamp, M. Steiner, H. Tietze-Jaensch, Physica B **241-243**, 570 (1998).

[3] D. Hinzke and U. Nowak, Phys. Rev. B **58**(1), 265 (1998).

[4] J. Ricardo de Sousa and J. A. Plascak, Phys. Lett. A **237**, 66 (1997).

[5] A. Mailhot, M.L. Plumer, and A. Caillé, Phys. Rev. B **48**, 15835 (1993).

[6] M.E.J. Newman and G.T. Barkema. *Monte Carlo Methods in Statistical Physics*. Oxford: Clarendon, 1999.

[7] D.P. Landau and Kurt Binder. *A Guide to Monte Carlo Simulations in Statistical Physics*. Cambridge: Cambridge University Press, 2000.

[8] K. Binder, K. Vollmayr et al., Internat. J. Modern Phys. C **3**(5), 1025 (1992).

[9] M. S. S. Challa and D. P. Landau, Phys. Rev. B **34**(3), 1841 (1986).

[10] A. M. Ferrenberg and R. H. Swendsen, Phys. Rev. Lett. **61**, 2635 (1988); A. M. Ferrenberg *Computer Simulation Studies in Condensed Matter Physics III*. Springer Proceedings in Physics, **53**. Heidelberg: Springer-Verlag, 1991.

[11] Kun Chen, PhD Thesis, University of Georgia, 1993.